This is a preprint, the final version is subject to change, of the American Mineralogist (MSA)
Cite as Authors (Year) Title. American Mineralogist, in press.
(DOI will not work until issue is live.) DOI: http://dx.doi.org/10.2138/am-2017-6132

Revision 2

Stability field of the Cl-rich scapolite marialite

Kaleo M. F. Almeida[1,2*]

David M. Jenkins[1]

[1] Department of Geological Sciences and Environmental Studies

Binghamton University

Binghamton, NY, 13902

[2] Present address: Department of Earth and Environmental Sciences, Rutgers University, Newark, NJ 07102

[*]Corresponding author

Abstract

Scapolites are widespread rock-forming aluminosilicates, appearing in metasomatic and igneous environments, and metamorphic terrains. Marialite ($Na_4Al_3Si_9O_{24}Cl$) is the Cl-rich end member of the group. Even though Cl-rich scapolite is presumably stable over a wide range of pressure and temperature, little is known about its stability field. Understanding Cl-rich scapolite paragenesis is important since it can help identifying subsurface fluid flow, metamorphic and isotopic equilibration. Due to its metasomatic nature Cl-rich scapolite is commonly reported in economic ore deposits, hence it is of critical interest to the mineral resource industries who seek to better understand processes contributing to mineralization. In this experimental study two reactions were investigated. The first one was the anhydrous reaction of albite + halite to form marialite ($3NaAlSi_3O_8 + NaCl = Na_4Al_3Si_9O_{24}Cl$ (1)). The second reaction was the hydrothermal equivalent described by $H_2O + Na_4Al_3Si_9O_{24}Cl = 3NaAlSi_3O_8$ + liquid (2), where the liquid is assumed to be a saline-rich hydrous-silicate melt. Experiments were performed using a piston-cylinder press and internally heated gas vessels. The temperature and pressure conditions range from 700-1050°C and 0.5-2.0 GPa, respectively. The starting materials were synthetic phases including end-member marialite, high-albite, and halite. For reaction (1), marialite was found to be stable above 920° to 990°C over a pressure range of 0.65 to 2.0 GPa, but unstable between 800° and 950°C at pressures of 0.5 GPa and lower. For reaction (2), marialite was found to be very intolerant of water, requiring a minimum bulk brine salinity of approximately 0.8 mole fraction of NaCl at 1050°C and 1000°C at pressures of 2.0 and 1.5 GPa, respectively. From the location of reaction (1) in pressure-temperature space thermochemical data for marialite were extracted. Values for the enthalpy of formation (ΔH_f^o) and third-law entropy ($S°$) for marialite at 298 K and 1 atm have been calculated as -12,167.5 ± 1.5 kJ/mole

and 0.7579 ± 0.002 kJ/K·mole, respectively, based on existing thermochemical data for high-albite and halite. The main implication of this study is that end-member marialite is only stable at temperatures greater than 920°C and pressures equivalent to a minimum depth of 18 km under extremely dry conditions. These conditions are not generally realized in typical scapolite-bearing rocks, which occur at shallower-levels and in hydrothermal settings, which may be why pure marialite is rarely observed. This study is the first experimentally determined stability for end-member marialite and provides an important reference for quantifying the stability of Cl-rich scapolites found in nature.

Keywords: Scapolite, marialite, marialite stability, chlorine, chloride brine, albite

Introduction:

Minerals in the scapolite group are widespread rock-forming aluminosilicates that display an extended range of solid solution. The scapolite mineral group can be thought of as the result of combining three moles of plagioclase with a salt (i.e. NaCl, $CaCO_3$, $CaSO_4$) (e.g., Evans et al., 1969; Goldsmith, 1976; Hassan and Buseck, 1988; Teertstra and Sherriff, 1997). They can be compositionally illustrated as a solid solution of four end-members: a sodium chloride end-member, marialite ($Na_3Al_3Si_9O_{24}$·NaCl), two calcium carbonate end-members, meionite ($Ca_3Al_6Si_6O_{24}$·$CaCO_3$) and mizzonite ($NaCa_3Al_5Si_7O_{24}CO_3$ = albite·2 anorthite·$CaCO_3$), and a calcium sulfate end-member, sulfate meionite or silvialite ($Ca_4Al_6Si_6O_{24}SO_4$) (Newton and Goldsmith, 1976; Teertstra et al. 1999). Unlike other chloride bearing minerals (such as amphiboles, apatites, and micas), scapolite usually contains little OH (Teertstra and Sherriff, 1997), hence its composition can be used as a tracer of the Cl and CO_2 contents of the fluid responsible for its formation, independent of the fugacity of H_2O (f_{H2O}) (Ellis, 1978; Rebbert and Rice, 1996; Filiberto et al., 2014).

Scapolites are commonly reported in nature over a wide range of temperature and pressure, and it is regarded as a typical metamorphic mineral, so long as the fluids necessary for its stability are present (Boivin and Camus, 1981; Teertstra and Sherriff, 1997). Even though Cl-rich scapolite is thought to be stable over a wide range of pressure and temperature, little is known about its stability field and scapolites approaching end-member marialite are rare or perhaps non-existent (e.g., Teertstra and Sherriff, 1997). It is of interest to note that scapolite has been identified in chondritic meteorites (Teertstra and Sherriff, 1997), and has been detected in SNC meteorites and on the surface of Mars via high-resolution reflectance spectra (Clark et al., 1990; Filiberto et al., 2014).

Fluid-composition-indicative minerals, such as scapolite, are critical for better understanding fluid flow events and metasomatic reactions leading to the formation of alteration minerals. Furthermore, they help to give insight into fluid pulses and their origins (Hammerli et al., 2013; Hammerli et al., 2014; Kusebauch et al., 2015). Halogens (Cl, F, Br, I) may be used to distinguish these fluids, as they are major anions in metasomatic fluids, but only minor or trace elements in bulk solid. Therefore, halogen concentrations and ratios in mineral phases that formed during metasomatic processes reveal characteristics of a fluid, rather than features inherited from the pristine solid (Pan and Dong, 2003; Hammerli et al., 2014; Kusebauch et at., 2015).

Several studies involving scapolite emphasize the role of fluids as active agents of prograde regional metamorphism. Mora and Valley (1989) suggest that fluid flow during metamorphism may control mineral reactions, enhance reaction rates, and enable transport of elements and heat. Metamorphic fluid-rock interaction can be monitored by mineral reaction progress or stable isotope data. Gradients in the activities of species (such as K^+, Na^+, F^-, Cl^-, or

88 CO_2) that are readily exchangeable with externally derived fluids may further constrain
89 metamorphic fluid-rock ratios (Mora and Valley, 1989; Oliver et al., 1992; Moecher, 1993).
90 Because Cl is strongly partitioned into aqueous fluids relative to solid phases, minerals that
91 concentrate Cl, such as scapolite, apatite, biotite, and amphibole, may be particularly sensitive
92 indicators of fluid-rock interaction.

93 Mora and Valley (1989) reported scapolite in greenschist through amphibolite-facies
94 metasedimentary rocks of the Proterozoic Belt Supergroup in northern Idaho. Interestingly,
95 more than 90% of the Cl-rich scapolite is stratigraphically controlled and distributed parallel to
96 bedding. This restricted presence of Cl-rich scapolite suggests that it crystallized during
97 regional metamorphism in rock layers that originally contained halite (Mora and Valley, 1989).
98 Similarly, Vanko and Bishop (1982) investigated the occurrence and origin of Cl-rich scapolite
99 in the Humboldt lopolith, northwest Nevada. The Humboldt lopolith is a large composite
100 middle Jurassic volcano-plutonic center of mafic composition with intense hydrothermal
101 alteration. The lopolith hosts large concentrations of Cu, Au, and other valuable elements
102 (Johnson and Barton, 2000). In the Humboldt lopolith scapolite occurs as a pervasive
103 replacement of plagioclase and other minerals in gabbro, diorite, and volcanic rocks, and also
104 occurs as a fracture-filling mineral along with analcime. Marialitic scapolite is widespread in
105 the lopolith interior. Electron probe micro-analysis (EPMA) shows that some scapolite in
106 gabbro contains up to 3.95 wt% Cl, out of a theoretical maximum of 4.2 wt% Cl (Vanko and
107 Bishop, 1982). Scapolitized rocks have up to 80 volume percent scapolite, indicating either a
108 dramatic influx of Na and Cl or the previous existence of halite in order for extensive Cl-rich
109 scapolite to occur. A possible source of Na and Cl is pre-existing evaporite beds derived from
110 the wallrocks (Vanko and Bishop, 1982). In both the Belt Supergroup and Humboldt lopolith

localities field evidence points to the role of halite, or at least significant amounts of chloride beyond what could be introduced in a typical magma, in stabilizing Cl-rich scapolite. Hence, it is of particular interest to determine the stability of end-member marialite in pressure-temperature-composition (*P*-*T*-*X*) space to establish the boundary conditions of this halogen-bearing mineral.

Much of our knowledge of the formation conditions of scapolite comes from the examination of their occurrence in various geological environments. Analyzed scapolites range from approximately 80% marialite (20% meionite) to 10% marialite (90% meionite), though most analyses cluster between 20 and 70 mol% marialite component (Goldsmith, 1976; Teertstra and Sherriff, 1997). Regardless of the location or composition of the rocks being replaced, scapolite commonly appears to occur as the result of a desiccation mechanism; in other words, during metamorphic fluid-rock interaction the fluids undergo a net salinity increase due to successive chemical evolution and consumption of a free fluid phase (Kullerud and Erambert, 1999). Several experimental studies, including those of Orville (1974), Ellis (1978), and Baker and Newton (1995), have focused on scapolite solid solutions. Orville (1974) determined that scapolite is stable relative to plagioclase + calcite + halite at 750°C and 0.4 GPa over the range of plagioclase composition from $Ab_{85}An_{15}$ to $Ab_{70}An_{30}$. Ellis (1978) determined that solid-solution scapolite is stable relative to plagioclase + calcite at 750°C and 0.4 GPa over the range of plagioclase compositions $Ab_{47}An_{53}$ to $Ab_{17}An_{83}$. Baker and Newton (1995) have investigated the stability field of scapolite, plagioclase, and calcite in the Cl-absent system $CaAl_2Si_2O_8$-$NaAlSi_3O_8$-$CaCO_3$ at 775-850°C and 0.7 GPa. Newton and Goldsmith (1976) reported *P*-*T* stability fields for end-members meionite and sulfate meionite and listed a few experiments pertaining to the stability of marialite but proposed no stability field for it.

Filiberto et al. (2014) proposed a *P-T* diagram for marialite based on various observations reported in the literature, but no systematic experimental study has been presented on end-member marialite.

This study investigates the stability field of marialite and how it changes as water is introduced to the system. The pressure and temperature range in which marialite is stable relative to albite and halite will be defined. Chlorine is known for its hydrophilic behavior, hence marialite is expected to destabilize in the presence of water (Selverstone and Sharp, 2015). This study will also define the stability of marialite at hydrothermal conditions. Additionally, establishing the reaction boundary:

$$3NaAlSi_3O_8 + NaCl = Na_4Al_3Si_9O_{24}Cl \quad (1)$$
albite halite marialite

enables the extraction of thermochemical data for marialite, in particular its enthalpy of formation (ΔH_f^o) and third-law entropy ($\Delta S°$), for which there are no extant data.

Methods

Starting materials

All phases were synthesized from appropriate mixtures of reagent-grade oxides, salt, and carbonate (SiO_2, Al_2O_3, NaCl, and Na_2CO_3). The SiO_2 was made by desiccating silicic acid by heating gradually to 1100°C in air overnight producing cristobalite. Care was taken to roast the reagent NaCl to at least 500°C in air for several hours to decrepitate aqueous fluid inclusions that are invariably present. After weighing and mixing the reagents Na_2CO_3, Al_2O_3, and SiO_2, they were heated in a furnace at 900°C for 15 minutes to remove CO_2. The NaCl was added following decarbonation. For hydrothermal experiments requiring very small amounts (< 2 wt%) of water, $Al(OH)_3$ was added in the appropriate amount which would then dehydrate to H_2O and Al_2O_3; the amount of additional Al_2O_3 added in this manner was considered a

158 negligible change to the bulk Al_2O_3 of a given mixture. The bulk compositions of all samples
159 investigated in this study are presented in Table 1.

160 **Sample treatment and high-pressure apparatus**

161 Starting mixtures were placed into sealed platinum and silver-palladium (Ag_{50}-Pd_{50})
162 capsules, which were made from tubing that was cleaned in acetone, flame-annealed to around
163 1,200°C, and then crimped. Platinum capsules were used for synthesis experiments and were
164 4.0 mm outer diameter (OD) by 15 mm length and wall thickness of 0.18 mm. Platinum or
165 Ag_{50}-Pd_{50} capsules were used for reversal experiments, depending on the conditions of
166 treatment, and were 1.5 mm OD by 10 mm length having wall thickness of 0.13 mm. The first
167 set of experiments focused on the synthesis of marialite and albite and about 50-60 mg of
168 sample was used. In subsequent reversal experiments, where all desired phases were present in a
169 reversal mixture, about 5 mg of sample was used. For all the experiments that were treated dry,
170 the capsules were put in a 160°C furnace in air for 15 minutes prior to sealing to ensure that all
171 the moisture was removed from the capsule. For hydrothermal experiments, water was
172 introduced in the form of $Al(OH)_3$, as mentioned above, and the capsule was crimped shut,
173 welded, and weighed. After completion of experiments the capsules were reweighed to check
174 that the capsule remained sealed. To obtain a successful yield of marialite, excess NaCl had to
175 be added to the starting mixture. To control the NaCl abundance in hydrothermal experiments,
176 excess NaCl in the synthetic marialite was removed by rinsing in deionized water. The mixture
177 was then analyzed by X-ray powder diffraction to check that there was no NaCl left and then
178 NaCl was reintroduced in known amounts to allow better precision in calculating brine
179 concentrations.

A $^{1}/_{2}$-inch diameter piston-cylinder press was used for experiments with pressures at and above 1.0 GPa with NaCl serving as the pressure medium and fitted with a straight graphite furnace and crushable MgO or NaCl inside of it. For experiments at 1.0 GPa with temperatures above 860°C the graphite sleeve was additionally fitted with an outer straight pyrex sleeve to prevent mechanical failure of the graphite furnace and crushable MgO spacers were used instead of NaCl. Temperatures ranged from 700 to 1050°C and were measured with a chromel-alumel thermocouple, which was placed in the salt pressure media right above the sample. Temperature uncertainties are estimated as ± 5°C for reversal experiments (using smaller capsules with the sample within 0.5 mm of the thermocouple tip) and ± 15°C for synthesis experiments (using larger capsules with the sample within 2-3 mm of the thermocouple tip). Pressures from 1.0-2.0 GPa have estimated uncertainties of 0.05 GPa. Experiments were brought up from room temperature to the target temperature using heating ramps of 0.5 to 2 minute; the heating rate is noted in this study because it may have some bearing on the relative nucleation rates of scapolite versus albite. After between 1 and 5 days, the piston-cylinder press was quenched and dismantled. The capsule was weighed, an incision was made into it, dried at 110°C, and weighed again to determine the free-water content within the capsule.

An internally heated gas vessel was used for the experiments performed at pressures below 1.0 GPa with argon as the pressure medium. Two Inconel®-sheathed chromel-alumel thermocouples were placed in the vessel to observe any temperature gradient along the capsule; gradients were generally 10°C or less with corresponding uncertainties in the average temperature of ± 5°C. Desired temperatures were reached in 3-5 minutes. Pressures were measured with both bourdon-tube and manganin-cell gauges and have an estimated uncertainty of 0.005 GPa.

Analytical methods

Powder X-Ray diffraction (XRD) analysis was perfomed using a Panalytical Xpert PW3040-MPD diffractometer. Samples were mounted on a zero-background single crystal quartz plate, with the operating settings at 40 kV and 20 mA using CuKα radiation and a diffracted-beam graphite monochromator. All of the samples were first analyzed in a continuous scan from 10 to 60° 2Θ with a step size of 0.020° at 1.0 second per step. Reaction direction was determined using the peak-area ratios of the largest peaks of marialite [(112), 25.8° 2Θ] and albite [($(\bar{2}02)$, 27.8° 2Θ] as a simple way of estimating the proportions of these phases. The Panalytical software HighScore® was used to calculate the area of selected X-ray peaks. Reaction-reversal starting mixtures, containing all of the desired phases, were mixed three times in an agate mortar using acetone to ensure a homogeneous mixture. These mixtures were then scanned from 20 to 31° 2Θ five times to obtain an average and standard deviation of the peak-area ratios for reference; reaction direction was then determined by comparing peak-area ratios observed in subsequent treatments of the starting mixture to these reference ratios. Unit-cell dimensions were determined by Rietveld structure refinement using the patterns collected from 10-60° 2Θ and the program GSAS (Larson and Von Dreele, 2000). The zero point of 2Θ was refined first using the NaCl (a_0 = 5.6401 Å) in the sample as an internal standard to account for differences in sample displacement from one scan to another. Refinements were initiated using the structures of marialite and albite reported by Sokolova et al. (1996) and Prewitt et al. (1976), respectively. Parameters that were refined included background, unit-cell dimensions, atomic coordinates, preferred orientation, and LX and LY terms in the profile function.

Electron probe micro-analysis (EPMA) was done on a JEOL 8900 Superprobe at Binghamton University. Samples were mounted in epoxy, polished to a final diamond grit size

of 0.5 μm, carbon coated, and analyzed using beam conditions of 15 kV and 10 nA. Analyses were conducted by counting 10 seconds on peaks and 3 seconds on background to minimize diffusion of Na under the electron beam. Matrix corrections were made using the atomic number, absorption, and fluorescence (ZAF) correction scheme (e.g., Reed, 1996, p. 134–140). The standards used were: albite for Na, palladium chloride ($PdCl_2$) for Cl, and pure oxides for Si and Al.

Results

Synthesis of starting phases

Starting phases were synthesized at approximately 1030°C and 1.8-1.9 GPa for 2 to 3 days. The bulk compositions of the mixtures used for this study and synthesis conditions are listed in Table 1. Two variables were initially considered to be important in obtaining high yields of marialite, namely the heating time from room temperature to the target temperature (i.e., ramp time) to minimize the nucleation of albite during heating, and the proportion of NaCl in the starting mixture. In general, NaCl had to be introduced in excess to produce a good yield of marialite (≥80 wt%) using ramp times of 0.5–1.0 min (i.e., heating rates of 343-172°C/s). Somewhat surprisingly the highest yield of marialite obtained was sample "MARF1 product" (Table 1), which was made at ≥ 1030°C and 1.8 GPa for 48 h with the longer ramp time. There is some quartz, albite, and halite present in the sample, but they are minor phases (<10%). This experiment differed from other experiments because there was another capsule (MARF1-2) placed just above it in the piston-cylinder press; most likely a temperature gradient was present and the true temperature was perhaps 10-30°C higher than the set-point value of 1030°C. The positive temperature gradient effect was probably the main reason for the strong marialite growth. For comparison, sample MARF1-10 had the same starting composition and was treated

at the same nominal conditions of 1030°C and 1.8 GPa for 48 h with a ramp time of 0.5 minutes, but was placed alone in the piston-cylinder press with the thermocouple next to the sample giving a more accurate (less underestimated) temperature. The resultant assemblage was predominantly albite (≥80%) with minor quartz and halite (with periclase as a contaminant from the pressure medium during sample recovery).

Typically, the synthetic marialite and albite are equant grains with sizes on the order of 10-20 μm and displaying no obvious reaction textures. The degree of Al-Si order/disorder in albite for this study has been determined using the $\Delta 2\Theta(131)$ measured from powder X-ray diffraction scans after Goldsmith and Jenkins (1985). The $\Delta(131)$ value for the albite in MARF1-10 is 1.91, which indicates it is high-albite.

Stability of marialite at dry conditions

Mixtures containing strong yields of marialite and albite were mixed together to acquire a well-seeded reversal mixture for investigating reaction (1). Equilibrium is, therefore, demonstrated by the growth of marialite at the expense of albite and halite with increasing temperature and vice versa with decreasing temperature with minimum influence from phase-nucleation kinetics. Table 2 lists the samples used to make the reversal mixtures.

A series of experiments at dry conditions was done over the range of 700-1050°C and 0.5-2.0 GPa for 1 to 5 days. The treatments at dry conditions for the reversal mixtures pertaining to reaction (1) are given in Table 3 and the results are shown Figure 1. The boundary that is shown is a straight-line interpretation of the experimental data fit “by eye”. The jadeite + quartz to albite (Holland, 1980) and the halite solid to liquid (Akella et al., 1969) transitions are also shown which constrain where reaction (1) may occur. This is the first experimentally determined location for the lower-thermal stability of end-member marialite.

The lower-pressure data shown in Figure 1 suggest that marialite is not stable below 0.6 GPa; however, the sense of reaction was less clear at these lower pressures making it difficult to accurately locate a lower-pressure stability boundary. This uncertainty in the lower-pressure stability of marialite is mentioned in the earlier literature. Marialite was first synthesized at 1 atm in the range of 770-850°C for durations of 80-450 hours by Eugster and Prostka (1960) and Eugster et al. (1962). It was later reported, in a personal communication to Orville (1975), that marialite broke down when heated for longer durations. Location of a boundary that is consistent with the data in Figure 1 and with Schreinemakers analysis of this system is presented below.

Stability of marialite at hydrothermal conditions

Introduction of water is expected to de-stabilize marialite as a result of the approximate reaction:

$$H_2O + Na_4Al_3Si_9O_{24}Cl = 3NaAlSi_3O_8 + H_2O\text{-}NaCl\text{-}NaAlSi_3O_8\text{-liquid} \quad (2)$$
water marialite albite $NaCl_l$

where $NaCl_l$ is a liquid that is probably rich in NaCl but with a minor amount of silicate as well as water dissolved in it, as suggested by Eugster and Protska (1960) and supported by the study of Makhluf et al. (2016) on the system $NaAlSi_3O_8$-H_2O-NaCl 1.0 GPa. Sample REVM6 was used for these hydrothermal experiments to investigate how tolerant the system is to water before marialite reacts to albite + $NaCl_l$, and how much it would impact its stability field. To have good precision for the brine concentration the NaCl was rinsed out of the sample and reintroduced in a known amount as discussed in the Methods section. After rinsing the REVM6 sample, about 2 mols of NaCl per mole of marialite was added to it, now called REVMR6. After a few experiments with similar results of complete albite growth, about 6 moles of NaCl was added to REVMR6, now called REVMS6, which presumably increased the NaCl content of

the $NaCl_l$ phase and stabilized marialite. Experiments at hydrothermal conditions were done over the range of 960-1050°C and 1.5-2.0 GPa varying in length from 1 to 3 days as given in Table 4. Figures 2a and 2b show the T- X_{NaCl}^{Bulk} diagrams at fixed pressures of 2.0 and 1.5 GPa, respectively, where X_{NaCl}^{Bulk} indicates the mole fraction of NaCl/(H_2O + NaCl) for the bulk mixture and may not necessarily be the true composition of the $NaCl_l$ phase. The estimated hydrothermal melting curves of halite extrapolated from lower-pressure results of Aranovich and Newton (1996) are shown.

Previous to these experiments the authors hypothesized that marialite would be stable as long as it was inside the halite-saturated field; however, the results show that marialite breaks down at much higher X_{NaCl}^{Bulk} values. In fact, marialite is very intolerant to water; it requires, for example, a minimum bulk salinity X_{NaCl}^{Bulk} of approximately 0.8 at 1050°C and 2.0 GPa (Figure 2a). The horizontal solid lines at the NaCl-rich side of Figures 2a,b show, for reference, the breakdown of marialite to albite + halite at water-absent (dry) conditions. It is clear that marialite does not remain stable all of the way over to the halite saturation curve as expected but breaks down to albite and presumably $NaCl_l$. The degree of order/disorder for the albite formed in reaction (2) was examined for sample REVMR6-1, which showed strong albite growth. The $\Delta(131)$ value for the albite in REVMR6-1 is 1.94, indicating it remained high-albite as was observed in the water-free experiments described above and is consistent with the high temperatures of these experiments (Goldsmith and Jenkins, 1985).

Marialite composition

Marialite compositions were determined via EPMA, and are listed in Table 5, to confirm the composition of the scapolite produced by reactions (1) and (2). The same approach for cation calculation used by Evans (1969), Lieftink et al. (1993), and Teertstra and Sherriff (1997)

was applied in this study. The formula of marialite was initially calculated by normalizing to Si + Al = 12 atoms per formula unit (apfu). The criteria for accepting the analysis was based on (1) the analytical weight-percent total from the EPMA analysis being above 80 wt%, which is well above the 65 wt% minimum determined by Giblin et al. (1993), and (2) the sum of all cations being 16.0 ± 0.3. It was difficult to obtain samples that obeyed the second criteria for the marialite, presumably because of rapid Na diffusion under the electron beam, even for the relatively short counting times used in this study. This diffusive loss of Na under the electron beam was also described by Vanko and Bishop (1982) and Hammerli et al., (2014) for the analysis of marialitic scapolite. Therefore, compositions could show a slight deficit in Na and corresponding relative increase in Al and Si.

The samples analyzed, REVM5-4 and REVMS6-12, were experiments done at dry and hydrothermal conditions, respectively, inside the stability field of marialite. Table 5 shows that the two samples have similar compositions and are close to ideal marialite, with minor depletion in Na and Al and enrichment in Si. The goal of this analysis was to check if there were any compositional differences between the dry and hydrothermal treatments. Rather than experiencing dissolution of some component, such as silica, from marialite, the scapolite formed under hydrothermal conditions may even be closer to the ideal composition than that formed under dry conditions.

Discussion

Marialite phase equilibria and thermodynamic properties

The proximity of reaction (1) to the halite solidus and the breakdown of marialite at low pressures and high temperatures (Fig. 1), suggests that the phase equilibria of marialite involves a NaCl-rich melt or liquid ($NaCl_l$) in addition to albite and halite. In the two-component system

343 NaCl-$NaAlSi_3O_8$ these four phases constitute an invariant assemblage. Using the method of
344 Schreinemakers (e.g., Ehlers, 1972) an invariant-point array was constructed qualitatively as a
345 function of pressure and temperature. So long as one univariant curve and reaction direction is
346 known (e.g., reaction 1), the relative positions of the other curves can be found qualitatively.
347 Figure 3 shows the array of univariant curves about an invariant point for the invariant
348 assemblage of phases shown in the lower right portion of the diagram. The composition of
349 $NaCl_l$ is estimated to be between marialite and NaCl but closer to NaCl in composition as
350 suggested by Eugster and Protska (1960). Each univariant boundary is labeled with the phase in
351 parenthesis that is absent from the reaction. The general orientation of the array is determined
352 by the location of reaction (1), which is the $NaCl_l$-absent reaction in the context of Figure 3.
353 This analysis allows to identify the array of univariant curves that occur in this system and to
354 estimate their location relative to the extant experimental results of this study in *P*-*T* space
355 (Figure 4). The invariant point is estimated as being at 820°C and 0.8 GPa.
356 Using the *P*-*T* experimental brackets for reaction (1), estimating heat capacity (C_P) data
357 for marialite from the data of Komada et al. (1996), using the (adjusted) volume of marialite
358 from Sokolova et al., (1996) and Kabalov et al. (1998), and incorporating the thermochemical
359 data of Holland and Powell (2011) for other phases, the enthalpy of formation (ΔH_f^o) and third-
360 law entropy ($S°$) of marialite at 298K and 1 atm can be derived. First, the C_P of end-member
361 marialite was derived from the data of Komada et al. (1996) as follows. Komada et al. (1996)
362 present C_P coefficients for five different scapolites ranging in meionite (Me) contents from Me_{28}
363 to Me_{88}. A C_P/R vs mol% meionite content plot was made in order to extrapolate the C_P
364 coefficients for end-member marialite from the meionite-rich samples at temperatures ranging
365 from 298-1000K (Figure 5). The intercepts of the straight-line fits give the C_P/R value for Me_0

(pure marialite) at each specific temperature and these are listed in Supplementary Data Table S-1. The resultant values of C_P/R for marialite were fitted to the 4-term heat-capacity equation used by Holland and Powell (2011) and the derived coefficients are given in Table 6. Second, albite was treated as high-albite in accordance with the Δ131 parameter indicating that albite was disordered (high) at all conditions investigated. Lastly, reaction (1), being a solid-solid reaction, is very sensitive to small changes in ΔV of the reaction. Without data on the thermal expansion (α) or compressibility (β) of end-member marialite, these terms were not included for any phase in the thermochemical analysis presented here, implying that ΔV of the reaction is constant over the *P*-*T* range of this study. As additional data on the physical properties of marialite become available this simplification should be revised. With these assumptions, the volume of marialite reported by Sokolova et al. (1996) and Kabalov et al. (1998) (329.2 cm^3/mol) was found to be too low, resulting in the wrong sense of ΔV and therefore ΔG of the reaction. A small increase in the marialite volume was required (330.35 cm^3/mol or 0.35% increase) to get the correct sense of reaction direction.

At equilibrium, the Gibbs free energy expression:

$$\Delta G_{P,T} = 0 = \Delta H^{o}_{P_0,T_0} - T\Delta S^{o}_{P_0,T_0} + \int_{T_0}^{T} \Delta C_P dT - T\int_{T_0}^{T} \frac{\Delta C_P}{T} dT + \int_{P_0}^{P} \Delta V dP \quad (3)$$

can be applied to the *P*-*T* conditions of each experimental bracket for the reaction (1) boundary where $\Delta G_{P,T} = 0$. Rearranging this expression gives:

$$-\Delta H^{o}_{P_0,T_0} + T\Delta S^{o}_{P_0,T_0} = G' = \int_{T_0}^{T} \Delta C_P dT - T\int_{T_0}^{T} \frac{\Delta C_P}{T} dT + \Delta V(P - P_0) \quad (4)$$

where the enthalpy ($\Delta H^{o}_{P_0,T_0}$) and entropy ($\Delta S^{o}_{P_0,T_0}$) of reaction at P_0 = 1 atm and T_0 = 298 K can be derived by plotting *G*' (right-hand side of equation 4) vs temperature. The $\Delta H^{o}_{P_0,T_0}$ and the $\Delta S^{o}_{P_0,T_0}$ are simply the negative of the intercept and the slope of the line, respectively. Figure 6a

shows the *G'* vs temperature plot and a linear regression to the boundary-limiting (bracketing) reversal experiments and resultant values of $\Delta H^{o}_{P_0,T_0}$ and $\Delta S^{o}_{P_0,T_0}$ of reaction. Using these values one can solve for the ΔH^{o}_{f} and *S*° of marialite as follows:

$$\Delta H^{o}_{f}(\text{Mari}) = \Delta H^{o}_{P_0,T_0}(\text{reaction}) + 3\cdot\Delta H^{o}_{f}(\text{Alb}) + \Delta H^{o}_{f}(\text{Hal}) \quad (5a)$$

$$S°(\text{Mari}) = \Delta S^{o}_{P_0,T_0}(\text{reaction}) + 3\cdot S°(\text{Alb}) + S°(\text{Hal}) \quad (5b)$$

with the resultant ΔH^{o}_{f} and *S*° at 298K and 1 atm being -12,167.5 ± 0.2 kJ/mole and 757.9 ± 0.2 J/K·mole, respectively. Figure 6b shows the calculated boundary for reaction (1) based on the data in Table 6. Figure 6b also compares the boundary from this study to that proposed by Filiberto et al. (2014), which, despite the limited information on which their boundary was based, is only off by about 90°C.

Marialite breakdown in the presence of water

The same theoretical analysis was done for reaction (2). In this case H_2O is present in the system and the Schreinemakers analysis is depicted for the ternary system albite-halite-H_2O in *T*-*X* space in Figure 7. The approximate orientation of this array can be determined using the high thermal stability of marialite along the degenerate $NaCl_l$- and H_2O-absent reaction. It is important to note that the composition of $NaCl_l$ (H_2O-NaCl-silicate-liquid) is a speculation, but is assumed to be close to halite because of its relatively low melting temperature and high solubility in water. However, some amount of silicate could well be present in this phase considering the extensive solubility of albite in H_2O at the high *P*-*T* conditions of this study, even in the presence of a considerable amount of NaCl which acts to reduce the solubility of albite (Makhluf et al., 2016). Also, it is important to note that the bulk composition (solid dots in Fig. 7) will migrate towards the H_2O vertex as more water is introduced to the system. The

410 H_2O-absent reaction is dashed because it would only exist if H_2O is not present as a separate
411 phase, a condition that may not be realized in the H_2O-rich portion of this array.
412 Fitting the Schreinemakers analysis of Figure 7 to the data in Figures 2a and 2b allows
413 the estimation of the position of the invariant point and array of univariant boundaries consistent
414 with the experimental results for the hydrothermal experiments done at 2.0 and 1.5 GPa, as
415 shown in Figures 8a and 8b, respectively. Figures 8a and 8b demonstrate how the stability of
416 marialite changes with increasing H_2O content. Starting at the ($NaCl_l$) reaction on the far right,
417 which is defined by the data from dry experiments in Figures 1 and 4, this implies that pure
418 marialite is extremely intolerant to water and breaks down to albite + $NaCl_l$ along the (Hal)
419 boundary at high mole fractions of NaCl. This breakdown occurs inside the halite liquidus curve
420 in the H_2O-NaCl system, as extrapolated from the lower-pressure data of Aranovich and
421 Newton (1996), suggesting that the eutectic melt is not simply halite in composition. The (Alb)
422 and (Mari) boundaries are dashed because there are very little data to define their location, and,
423 as mentioned above, the (H_2O) dash-dot boundary is only stable if an H_2O-rich phase is not
424 present. Based largely on the intersection of (Hal) and ($NaCl_l$) boundaries, the locations of the
425 invariant points are estimated to be at 990°C and 0.85 $X_{\mathrm{NaCl}}^{\mathrm{Bulk}}$ at 2.0 GPa, and 945°C and 0.92
426 $X_{\mathrm{NaCl}}^{\mathrm{Bulk}}$ at 1.5 GPa. Vanko and Bishop (1982) also found that high salinities were necessary to
427 stabilize marialitic scapolite (~ 0.18 X_{AnEquiv}), requiring a minimum salinity of 50 mol% NaCl at
428 700-750°C. From this study, it appears that end-member marialite requires even higher
429 salinities.
430 Due to the limited knowledge of the composition of the $NaCl_l$ phase and corresponding
431 lack of thermochemical data, a thermodynamic analysis of the hydrothermal experiments was
432 not done.

Implications

Comparison of the results of this study to Cl-rich scapolite reported in the literature may help shed light on the minimum brine concentration as well as pressure and temperature required for the formation of Cl-rich scapolites found in nature. Regarding composition, Figure 9 shows the wide range of solid solution displayed by scapolites reported in nature, with representative samples from the hydrothermally altered Humboldt Lopolith, Nevada, (Vanko and Bishop, 1982), amphibolite-facies calc-silicates from northwestern Queensland, Australia (Oliver et al, 1992), scapolites occurring within melt inclusions in augite from the Nakhla (Martian) meteorite (Filiberto et al., 2014), and from a variety of geological localities meant to represent the range of natural scapolites (Graziani and Lucchesi, 1982). Shown for comparison are the average compositions of the marialite samples made here (Table 6), where the equivalent anorthite content is defined here as the molar ratio of Ca/(Na + Ca). The samples made in this study have Cl values that are similar to other terrestrial and Martian samples but lack any meionite or mizzonite component, and, therefore, closely approximate ideal marialite. Results from this study should provide insights into the origins of the most Cl-rich scapolites.

Comparing the thermal stability of marialite determined in this study with previous experimental studies of scapolite suggests that small changes in scapolite composition from end-member marialite causes a substantial shift in its stability relative to the plagioclase plus salt assemblage. Considering the high-temperature experimental brackets for the water-free system involving pure marialite (reaction 1) from this study, and comparing them to the high-temperature stability of meionite reported by Newton and Goldsmith (1976), along with much lower-temperature stabilities of intermediate-composition scapolites reported by Orville (1974), Ellis (1978), Oterdoom and Gunter (1983), and Baker and Newton (1995), it can be concluded

that intermediate scapolite has a lower thermal stability compared to marialite and meionite. Additional experimental work on the *P-T-X* stability of an intermediate scapolite has been reported (Almeida and Jenkins, 2016) suggesting the presence of a low-temperature eutectoid-type stability for intermediate scapolite coexisting with albitic and anorthitic plagioclase as proposed for carbonate scapolites (e.g., Baker and Newton, 1995). This may indicate part of the reason why end-member scapolite is not found on Earth; marialite and meionite require temperatures and pressures attained at mid to lower crustal levels while, by comparison, intermediate composition scapolite is stable over a wider range of pressure and temperatures. The implication is that it is intermediate scapolite that is commonly reported in shallower-level and more accessible metasomatic environments and metamorphic terrains.

Fluid-rock interaction events are commonly accompanied by the formation of economic mineral deposits, which provides an excellent context for investigation of the halogens present in the fluid responsible for the hydrothermal alteration and ore metal transportation (Pan and Dong, 2003; Hammerli et al., 2014; Hammerli et al., 2015; Kusebauch et al., 2015). Chlorine has the tendency to strongly partition into the aqueous fluids relative to solid phases; therefore Cl-rich scapolite may be used as a sensitive indicator of fluid-rock interaction (Mora and Valley, 1989). The hydrothermal experiments involving end-member marialite (reaction 2) from this study indicate that marialite is very intolerant to water. For pure marialite to be stable in the $NaAlSi_3O_8$-NaCl-H_2O system, a minimum temperature of 900°C at 1.0 GPa is needed, while the minimum bulk salinity of the assemblage must be 0.8 X_{NaCl}^{Bulk} at 1050°C and 1000°C under pressures of 2.0 GPa and 1.5 GPa, respectively (Figs. 8a,b). Such a high mole fraction of NaCl is probably above the saturation level of halite in the H_2O-NaCl system. The necessity of a high concentration of NaCl and high temperatures to stabilize marialite suggests, at the very least,

that end-member marialite is a mineral equivalent to high-temperature metamorphic conditions (granulite facies), meaning it is a "dry" mineral, and it would not be likely to have a hydrothermal origin. Because progressive metamorphism tends to cause the dissolution of halite by devolatilization reactions (e.g., Oliver et al. 1992), reaching the high temperature and high $X_{\mathrm{NaCl}}^{\mathrm{Bulk}}$ conditions required for stabilizing pure marialite is rarely obtained and can account for its absence in nature. Finally, the implication of this study is that the formation of veins, dikes, or meta-sedimentary sequences with high modal proportions of Cl-rich scapolite (e.g., Vanko and Bishop, 1982; Mora and Valley, 1989; Oliver et al., 1992) is less likely the result of channelized fluid flow and more likely the result of *in situ* formation under fluid-poor conditions.

Acknowledgments

The authors are grateful for the very careful and insightful reviews of Christof Kusebauch, Johannes Hammerli, and Associate Editor Callum Hetherington resulting in a much more refined manuscript. David Collins assisted with the electron microprobe analyses. Thanks go to David Vanko for providing information on the synthesis of marialite. Financial support for this study comes from NSF grant EAR-1347463 to DMJ.

References Cited

Akella, J., Vaidya, S.N., and Kennedy, G.C. (1969) Melting of sodium chloride at pressures to 65 kbar. Physical Review, 185, 1135-1140.

Almeida, K., and D. M. Jenkins (2016) A comparison between the stability field of a Cl-rich scapolite and the end-member marialite. Geological Society of America Abstracts with Programs, 48(7), abstract 313-5, doi: 10.1130/abs/2016AM-279255.

Aranovich, L.Y., and Newton, R.C. (1996) H_2O activity in concentrated NaCl solutions at high pressures and temperatures measured by the brucite-periclase equilibrium. Contributions to Mineralogy and Petrology, 125, 200-212.

Baker, J., and Newton, R.C. (1995) Experimentally determined activity-composition relations for Ca-rich scapolite in the system $CaAl_2Si_2O_8$-$NaAlSi_3O_8$-$CaCO_3$ at 7 kbar. American Mineralogist, 80, 744-751.

Boivin, P., and Camus, G. (1981) Igneous scapolite-bearing associations in the Chaine des Puys, Massif Central (France) and Atakor (Hoggar, Algeria). Contributions to Mineralogy and Petrology, 77, 365-375.

Clark, R. N., Swayze, G. A., Singer, R. B., and Pollack, J. B. (1990) High-resolution reflectance spectra of Mars in the 2.3-μm Region: Evidence for the mineral scapolite. Journal of Geophysical Research, 95, 14463-14480.

Ehlers, E.G. (1972) The interpretation of geological phase diagrams. Freeman and Company, San Franciso.

Ellis D.E. (1978) Stability and phase equilibria of chloride and carbonate bearing scapolites at 750°C and 4000 bar. Geochimica et Cosmochimica Acta, 42, 1271-1281.

Eugster, H.P., and Prostka, H.J. (1960) Synthetic scapolites. Geological Society of America Bulletin, 71, 1859-1860.

Eugster, H.P., Prostka, H.J., and Appleman, D.E. (1962) Unit-cell dimensions of natural and synthetic scapolites. Science, 137, 853-854.

Evans, B.W., Shaw, D.M., and Haughton, D.R. (1969) Scapolite stoichiometry. Contributions to Mineralogy and Petrology, 24, 293-305.

Filiberto, J., Treiman, A.H., Giesting, P.A., Goodrich, C.A., and Gross, J. (2014) High-temperature chlorine-rich fluid in the martian crust: A precursor to habitability. Earth and Planetary Science Letters, 401, 110-115.

Giblin, L.E., Blackburn, W.H., and Jenkins, D.M. (1993) X-ray continuum discrimination technique for the energy dispersive analysis of fine particles. Analytical Chemistry, 65, 3576-3580.

Goldsmith, J.R. (1976) Scapolites, granulites, and volatiles in the lower crust. Geological Society of America, 87, no. 2, 161-168.

Goldsmith, J.R., and Jenkins, D.M. (1985) The high-low albite relations revealed by reversal of degree of order at high pressures. American Mineralogist, 70, 911-923.

Graziani, G., and Lucchesi, S. (1982) The thermal behavior of scapolites. American Mineralogist, 67, 1229-1241.

Hammerli, J., Rusk, B., Spandler, C., Emsbo, P., Oliver, N. H. S. (2013) In situ quantification of Br and Cl in minerals and fluid inclusions by LA-ICP-MS: A powerful tool to identify fluid sources. Chemical Geology, 337-338, 75-87.

Hammerli, J., Spandler, C., Oliver, N. H. S., and Rusk, B. (2014) Cl/Br of scapolite as a fluid tracer in the earth's crust: insights into fluid sources in the Mary Kathleen Fold Belt, Mt. Isa Inlier, Australia. Journal of Metamorphic Geology, 32,93-112.

Hammerli, J., Spandler, C., Oliver, N. H. S., Sossi, P. Dipple, G. M. (2015) Zn and Pb mobility during metamorphism of sedimentary rocks and potential implications for some base metal deposits. Mineralium Deposita, 50, 657-664.

Hassan, I., and Buseck, P. R. (1988) HRTEM characterization of scapolite solid solutions. American Mineralogist, 73, 119-134.

Holland, T.J.B. (1980) The reaction albite = jadeite + quartz determined experimentally in the range 600-1200°C. American Mineralogist, 65, 129-134.

Holland, T.J.B., and Powell, R. (2011) An improved and extended internally consistent thermodynamic dataset for phases of petrological interest, involving a new equation of state for solids. Journal of Metamorphic Geology, 29, 333-383.

Johnson, D.A., and Barton, M.D. (2000) Field trip day four: Buena Vista Hills, Humboldt Mafic Complex, Western Nevada. Society of Economic Geologists Guidebook Series, 32, 145-162.

Johnson, D.A., and Barton, M.D. (2000) Time-space development of an external brine dominated, igneous-driven hydrothermal system: Humboldt mafic complex, western Nevada. Society of Economic Geologists Guidebook Series, 32, 127-143.

Kabalov, Y.K., Sokolova, E.V., Sherriff, B.L., and Jenkins, D.M. (1998) Refinement of the crystal structure of synthetic marialite. Crystallography Reports, 43, 578-583.

Komada, N., Moecher, D.P., Westrum Jr., E.F., Hemingway, B.S., Zolotov, M.Y., Semenov, Y.V., and Khodakovsky, I.L. (1996) Thermodynamic properties of scapolites at temperatures ranging from 10 K to 1000 K[a]. Journal Chem. Thermodynamics, 28, 941-973.

Kullerud, K., and Erambert, M. (1999) Cl-scapolite, Cl-amphibole, and plagioclase equilibria in ductile shear zones at Nusfjord, Lofoten, Norway: Implications for fluid compositional evolution during fluid-mineral interaction in the deep crust. Geochimica et Cosmochimica Acta, 63, 3829-3844.

Kusebauch, C., John, T., Barnes, J.D., Klügel, A., and Austrheim, H.O. (2015) Halogen element and stable chlorine isotope fractionation caused by fluid-rock interaction (Bamble Sector, SE Norway). Journal of Petrology, 56, 299-324.

Larson, A.C., and Von Dreele, R.B. (2000) General Structure Analysis System (GSAS), Los Alamos National Lab Report (LAUR) 86-748.

Lieftink, D.J., Nijland, T.G., and Maijer, C. (1993) Cl-rich scapolite from Odegardens Verk, Bamble, Norway. Norsk Geologisk Tidsskrift, 73, 55-57.

Makhluf, A.R., Newton, R.C., and Manning, C.E. (2016) Hydrous albite magmas at lower crustal pressure: new results on liquidus H_2O content, solubility, and H_2O activity in the system $NaAlSi_3O_8$–H_2O–NaCl at 1.0 GPa. Contributions to Mineralogy and Petrology, 171, 75, 18pp, DOI 10.1007/s00410-016-1286-0.

Moecher, D.P. (1993) Scapolite phase equilibria and carbon isotopes: constraints on the nature and distribution of CO_2 in the lower continental crust. Chemical Geology, 108, 163-179.

Mora, C.I., and Valley, J.W. (1989) Halogen-rich scapolite and biotite: Implications for metamorphic fluid-rock interaction. American Mineralogist, 74, 721-737.

Newton, R.C., and Goldsmith, J.R. (1976) Stability of the end-member scapolites: $3NaAlSi_3O_8 \cdot NaCl$, $3CaAl_2Si_2O_8 \cdot CaCO_3$, $3CaAl_2Si_2O_8 \cdot CaSO_4$. Zeitschrift fur Kristallographie, 143, 333-353.

Oliver, N.H.S., Wall, V.J., and Cartwright, I. (1992) Internal control of fluid compositions in amphibolite-facies scapolitic calc-silicates, Mary Kathleen, Australia. Contributions to Mineralogy and Petrology, 111, 94-112.

Orville, P.M. (1975) Stability of scapolite in the system Ab-An-Nacl-$CaCO_3$ at 4 kb and 750°C. Geochimica et Cosmochimica Acta, 39, 1091-1105.

Oterdoom, W.H., and Gunter, W.D. (1983) Activity models for plagioclase and $CO_3 \cdot$scapolites – An analysis of field and laboratory data. American Journal of Science, 283-A, 255-282.

Pan, Y., and Dong, P. (2003) Bromine in scapolite-group minerals and sodalite: XRF microprobe analysis, exchange experiments, and application to skarn deposits. Canadian Mineralogist, 41, 529-540.

Pitzer K.S., and Simonson, J.M. (1986) Thermodynamics of multicomponent, miscible ionic systems: theory and equations. Journal of Physical Chemistry, 90, 3005-3009.

Prewitt, C.T., Sueno, S., and Papike, J.J. (1976) The crystal structures of high albite and monalbite at high temperatures. American Mineralogist, 61, 1213-1225.

Rebbert, C.R., and Rice, J.M. (1996) Scapolite-plagioclase exchange: Cl-CO_3 scapolite solution chemistry and implications for peristerite plagioclase. Geochimica et Cosmochimica Acta, 61, 555-567.

Reed, S.J.B. (1996) Electron microprobe analysis and scanning electron microscopy in geology. Cambridge University Press, Cambridge, United Kingdom.

Selverstone, J., and Sharp, Z.D. (2015) Chlorine isotope behavior during prograde metamorphism of sedimentary rocks. Earth and Planetary Science Letters, 417, 120-131.

Sokolova, E.V., Kabalov, Y.K., Sherriff, B.L., Teertstra, D.K., Jenkins, D.M., Kunath-Fandrei, G., Goetz, S., and Jäger, C. (1996) Marialite: Rietveld-structure refinement and ^{29}Si MAS and ^{27}Al satellite transition NMR spectroscopy. Canadian Mineralogist, 34, 1039-1050.

Teertstra, D.K., and Sherriff, B.L. (1997) Substitutional mechanisms, compositional trends and the end-member formulae of scapolite. Chemical Geology, 136, 233-260.

Teertstra, D. K., Schindler, M., Sherriff, B.L., and Hawthorne, F.C. (1999) Silvialite, a new sulfate-dominant member of the scapolite group with an Al-Si composition near the *I*4/m-*P*4_2/n phase transition. Mineralogical Magazine, 63, 321-329.

612 Vanko, D.A., and Bishop, F.C. (1982) Occurrence and origin of marialitic scapolite in the
613 Humboldt lopolith, N.W. Nevada. Contributions to Mineralogy and Petrology, 81, 277-289.
614

615 Table 1. Mixture bulk compositions, treatment conditions, and products of phase synthesis
616 experiments.

Sample code	Bulk composition used	T (°C)	P (GPa)	t (h)	Products and comments
Marialite synthesis					
MARF1-1P	$Na_3Al_3Si_9O_{24}$ + 10.3NaCl	1030**	1.8	48	mari, hal, qtz
MARF1 product*	$Na_3Al_3Si_9O_{24}$ + 2NaCl	≥1030**	1.8	48	mari, alb, hal, qtz
MARF1-2*	$Na_3Al_3Si_9O_{24}$ + 10.3NaCl	1030**	1.8	48	mari, hal, alb, qtz
Albite synthesis					
MARF1-10	$Na_3Al_3Si_9O_{24}$ + 2NaCl	1030	1.8	48	alb, qtz, hal, peri (from pressure assemblage)
MARF2-10	$Na_3Al_3Si_9O_{24}$ + 4NaCl	1030	1.8	48	alb, qtz, mari, hal
Mari #1	$Na_3Al_3Si_9O_{24}$ + 2.6NaCl^	1030	1.8	72	alb, qtz, hal
Mari #3	$Na_3Al_3Si_9O_{24}$ + 2.6NaCl	1030	1.8	72	alb, qtz, hal
Fused mari #1-2	$Na_4Al_3Si_9O_{24}Cl$ + 4NaCl	1030	1.9	48	alb, hal, qtz

617 * Capsules were treated in the same experiment

618 ** Heating ramp time of 1 min used for these samples, all others were 0.5 min.

619 ^ NaCl was roasted to 900°C to drive off any fluid in inclusions

620 Abbreviations: alb = albite; hal = halite; mari = marialite; peri = periclase; qtz=quartz;

621 Note: MARF1 product and MARF1-10 have the same starting composition, but yielded
622 different phases. MARF1 product is thought to have yielded marialite due to being placed with
623 another capsule in the piston-cylinder press and being subjected to temperatures estimated to be
624 10-30°C higher than the setpoint of 1030°C.

625

626 Table 2. Synthetic phases used to make reversal mixtures for reaction (1).

Reversal mixture	Marialite	Albite	Halite* (moles)
REVM3	MARF1-1P	MARF1-10	6
REVM4	MARF1-1P	MARF1-10	6
REVM5	MARF1-2	Mari #3	6.5
REVM6	MARF1 product	Mari #3	2.5
REVMR6	MARF1 product	Mari #3	2
REVMS6	MARF1 product	Mari #3	8

627 * Moles of halite per mole of marialite

628

This is a preprint, the final version is subject to change, of the American Mineralogist (MSA)
Cite as Authors (Year) Title. American Mineralogist, in press.
(DOI will not work until issue is live.) DOI: http://dx.doi.org/10.2138/am-2017-6132

629 Table 3. Treatment at dry conditions of reversal mixtures for reaction (1).

Sample code	T (°C)	P (GPa)	t (h)	Products and comments
REVM4-2	800	0.50	48.5	no apparent reaction
REVM4-4	850	0.50	68	alb, mari, hal
REVM4-5	900	0.50	65	no apparent reaction
REVM4-9	920	0.50	64	no apparent reaction
REVM4-11	930	0.50	88	alb, hal, mari
REVM4-8	950	0.50	87	alb, mari, hal
REVM5-18	800	0.61	72	alb, mari, hal
REVM5-13	860	0.62	48.5	alb, mari, hal
REVM5-12	930	0.64	25	mari, alb, hal
REVM5-2	920	0.65	91	mari, alb, hal
REVM5-17	880	0.67	72	no apparent reaction
REVM5-19	900	0.67	42	no apparent reaction
REVM3-14	850**	1.0	88	alb, mari, hal
REVM4-3	860**	1.0	90	no apparent reaction
REVM4-6	870**	1.0	48	no apparent reaction
REVM5-10	880***	1.0	24	no apparent reaction
REVM4-7	890***	1.0	20	experiment failed after ~ 20 hours - no apparent reaction
REVM4-10	890***	1.0	48	no apparent reaction
REVM5-1	900***	1.0	64	mari, alb, hal
REVM5-3	910***	1.0	48	mari, alb, hal
REVM5-7	920***	1.0	48	mari, alb, hal
REVM3-2	700**	1.5	86	alb, mari, hal
REVM3-1	800**	1.5	72	alb, mari, hal
REVM3-3	850**	1.5	120	alb, hal, mari
REVM3-4	875**	1.5	120	alb, mari, hal
REVM3-5	885**	1.5	117	alb, mari, hal
REVM3-6	900**	1.5	120	alb, mari, hal
REVM3-9	930**	1.5	72	alb, mari, hal

REVM3-10	940**	1.5	92	alb, hal, mari
REVM3-12	945**	1.5	88	mari, hal, alb
REVM3-7	950**	1.5	76	mari, alb, hal
REVM3-11	960**	1.5	66	mari, hal, alb
REVM5-9	950**	2.0	24	alb, hal, mari
REVM5-11	980**	2.0	24	alb, mari, hal
REVM5-16	990**	2.0	21	mari, alb, hal
REVM5-14	1000**	2.0	24	mari, alb, hal
REVM5-4	1030**	2.0	48	mari, hal, alb
REVM5-8	1050***	2.0	24	complete mari

** Heating ramp of 1 min

*** Heating ramp of 2 mins

633 Table 4. Treatment at hydrothermal conditions of reversal mixtures for reaction (2).

Sample code	T (°C)	P (GPa)	t (h)	H_2O (wt%)	Products and comments
REVMR6-1	960*	1.5	42	2	complete alb
REVMS6-1	960*	1.5	20	2	alb, mari, hal
REVMS6-9	960*	1.5	23	1	no apparent reaction
REVMS6-16	960*	1.5	21	0.5	no apparent reaction
REVMS6-2	980*	1.5	20	1	mari, hal, alb
REVMS6-3	980*	1.5	68	2	complete mari
REVMS6-5	980*	1.5	21	2.5	alb, hal, mari
REVMS6-4	980*	1.5	21	3	complete alb
REVMR6-3	1000**	1.5	21	2	complete alb
REVMS6-6	1000*	1.5	20	2.5	mari, hal, alb
REVMS6-7	1000*	1.5	20	3	mari, hal, alb
REVMS6-8	1000*	1.5	22	3.5	complete alb
REVMS6-15	1000*	2.0	20	1	mari, hal, alb
REVMR6-4	1000*	2.0	21	2	complete alb
REVMS6-17	1000*	2.0	23	2	mari, hal, alb
REVMS6-18	1000*	2.0	22	3	alb, hal, mari
REVMS6-13	1010*	2.0	24	1	mari, hal, alb
REVMS6-10	1030**	2.0	20	2	mari, hal, alb
REVMS6-12	1030**	2.0	20	2.5	complete mari
REVMS6-11	1030**	2.0	22	3	alb, mari, hal
REVMS6-14	1050**	2.0	20	3	mari, alb, hal

634 * Heating ramp of 1 min

635 ** Heating ramp of 2 mins

636

637

638 Table 5. Compositions of marialite synthesized at dry and hydrothermal conditions in this study,
639 reported as weight% oxides and chlorine and cations per 12 Al+Si atoms for the average of *n*
640 electron microprobe analyses. Uncertainties (1σ) are given in parentheses.

Sample wt%	REVM5-4 (dry)	REVMS6-12 (hydrothermal)	Theoretical
n	5	6	---
SiO_2	69.1 (1.5)	65.6 (1.31)	64.0
Al_2O_3	17.2 (0.4)	16.92 (0.62)	18.1
Na_2O	13.7 (0.2)	13.74 (0.57)	14.7
Cl	4.12 (0.13)	4.61 (1.2)	4.2
Total	104.1 (1.8)	100.9 (1.66)	101.0
Total -O=Cl	103.3 (1.8)	99.88 (1.66)	100.0
Cations			
TSi	9.11 (0.05)	9.07 (0.07)	9.0
TAl	2.89 (0.05)	2.93 (0.07)	3.0
Sum T	12.00	12.00	12.0
Na	3.78 (0.06)	3.92 (0.2)	4.0
Anions			
Cl	0.99 (0.03)	1.15 (0.32)	1.0

641
642

643 Table 6. Thermochemical data used in this study from Holland and Powell (2011) and
644 thermochemical data derived from this study for marialite.

Phase	$\Delta H^\circ_{298K, 1bar}$ (kJ/mol)	$S^\circ_{298K, 1bar}$ (kJ/K·mol)	$V_{298K, 1bar}$ (kJ/kbar·mol)	a*	b (x10^5)	c	d
high-albite	-3921.49	0.2243	10.105	0.4520	-1.3364	-1275.9	-3.9536
halite (s)	-411.3	0.0721	2.702	0.0452	1.797	0	0
marialite	-12167.49	0.75793	33.035	1.172	9.0626	-4676.4	-8.2379

645 * The heat capacity terms (a, b, c, and d) are the coefficients in the expression $C_P = a + b(T) +$
646 $c/(T^2) + d/(T^{0.5})$, and have units that give the heat capacity (C_P) in kJ/K·mol.
647
648
649 Figure Captions
650 Figure 1. *P-T* diagram of the higher-pressure results of marialite (Mari) stability. Halite liquidus
651 from Akella et al., (1969). Jadeite (Jad) + quartz (Qtz) breakdown to albite (Alb) from
652 Holland (1980). Open circles indicate growth of albite; solid circles indicate growth of
653 marialite, and half-filled circles indicate no obvious reaction.
654 Figure 2. (a) Thermal stability of marialite in the presence of water (bulk H_2O wt% indicated) at
655 2.0 GPa, where X^{Bulk}_{NaCl} indicates the mole fraction of NaCl/(H_2O + NaCl) for the bulk mixture
656 and not necessarily for $NaCl_l$ (= H_2O-NaCl-silicate-liquid). Estimated hydrothermal melting
657 of NaCl extrapolated from lower-pressure results of Aranovich and Newton (1996). Short
658 horizontal line is the lower-thermal stability of marialite from Figure 1 extrapolated a short
659 distance into this diagram. (b) Stability of marialite in the presence of water at 1.5 GPa. Other
660 abbreviations and symbols as in Figure 1.
661 Figure 3. Schreinemakers analysis of the NaCl-$NaAlSi_3O_8$ binary join. Each divariant field is
662 labeled with the phases that coexist for the bulk composition (solid dot) investigated in this

study and the chemographic diagram of possible phase assemblages. Each univariant reaction boundary is labeled with the phase in parentheses that is absent from the invariant assemblage.

Figure 4. Data from Figure 1 with the calculated location of reaction (1) ($NaCl_l$) as described in the text along with the estimated locations of the other reaction boundaries based on Schreinemakers analysis.

Figure 5. Marialite (Me_0) C_P/R data extrapolated from straight-line fits to the scapolite data from Komada et al. (1996). Heat-capacity measurements were made at temperatures ranging from 298-1000K. Heat-capacity expression for marialite given in Table 6.

Figure 6. (a) *G*' vs *T* plot for reaction (1). Enthalpy and entropy of marialite are calculated using the derived $\Delta H°$ and $\Delta S°$ of reaction, which are the negative of the intercept and slope of the line, respectively. (b) Calculated location of reaction (1) based on the thermochemical values derived in this study (Table 8).

Figure 7. Reaction boundaries resulting from Schreinemakers analysis of the ternary system $NaAlSi_3O_8$-NaCl-H_2O plotted in *T*-*X*(wt% H_2O) space and labeled with the phase in parentheses that is absent from the invariant assemblage. The chemography of the invariant assemblage is shown in the upper-left ternary plot using the same abbreviations as in previous figures. The dots represent the bulk compositions investigated, while the stable divariant assemblages can be determined from the three-phase assemblages comprising the bulk composition in any sector. The H_2O-absent reaction is dashed (i.e., metastable) because it would only be stable if there is no separate H_2O-rich phase present at these conditions.

Figure 8. (a) Locations of univariant boundaries derived via Schreinemakers analysis in Figure 7 constrained by the hydrothermal experimental data at 2.0 GPa from Figure 2a. Short horizontal line is the lower-thermal stability of marialite from Figure 1 extrapolated a short

686 distance into this diagram. (b) Same analysis of the hydrothermal data at 1.5 GPa from Figure
687 2b. Estimated hydrothermal melting of NaCl at both pressures was extrapolated from lower-
688 pressure results of Aranovich and Newton (1996).

689 Figure 9. Chlorine contents in atoms per formula unit (apfu) versus mole fraction of the
690 equivalent anorthite content (An Equiv) of representative scapolites found in terrestrial
691 localities (Humboldt lopolith, Nevada, Vanko and Bishop, 1982; calc-silicates from NW
692 Queensland, Oliver et al., 1992; various geological settings, Graziani and Lucchesi, 1982) and
693 in the Nakhla Martian meteorite (Filiberto et al., 2014). The An Equiv values are those
694 reported in the original sources; for this study these values are defined as the molar ratio of
695 Ca/(Ca + Na).

696 Figure 1.

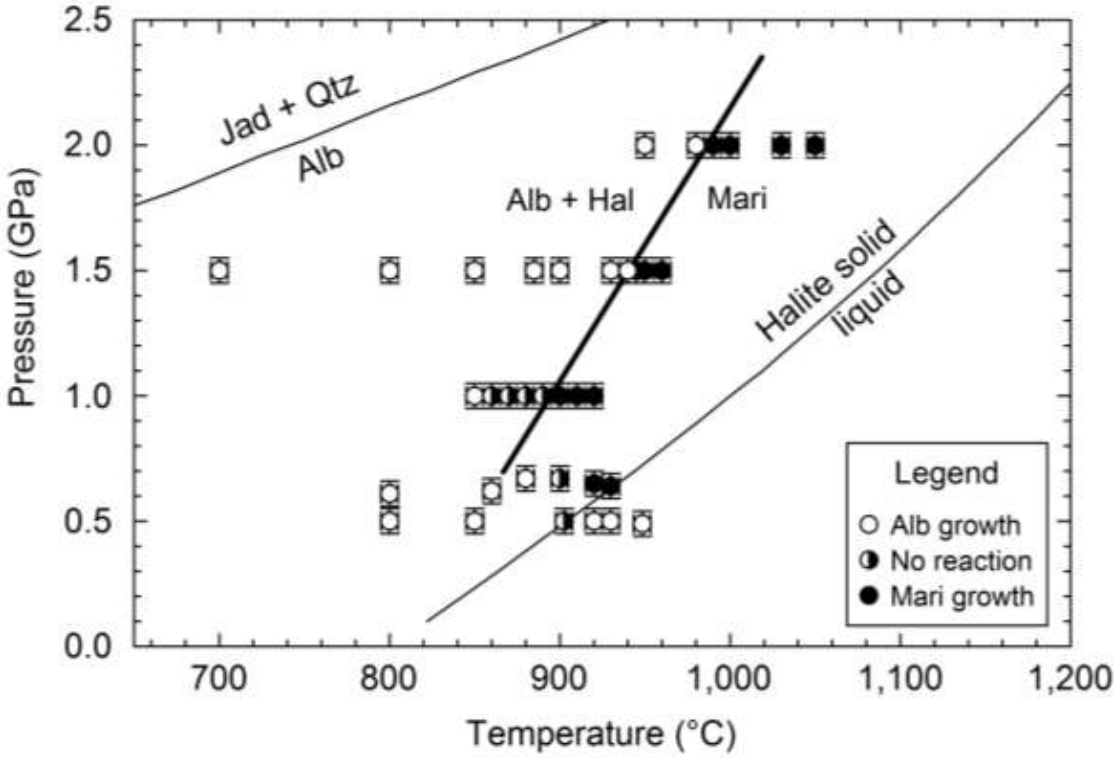

697
698
699

700 Figure 2. a,b

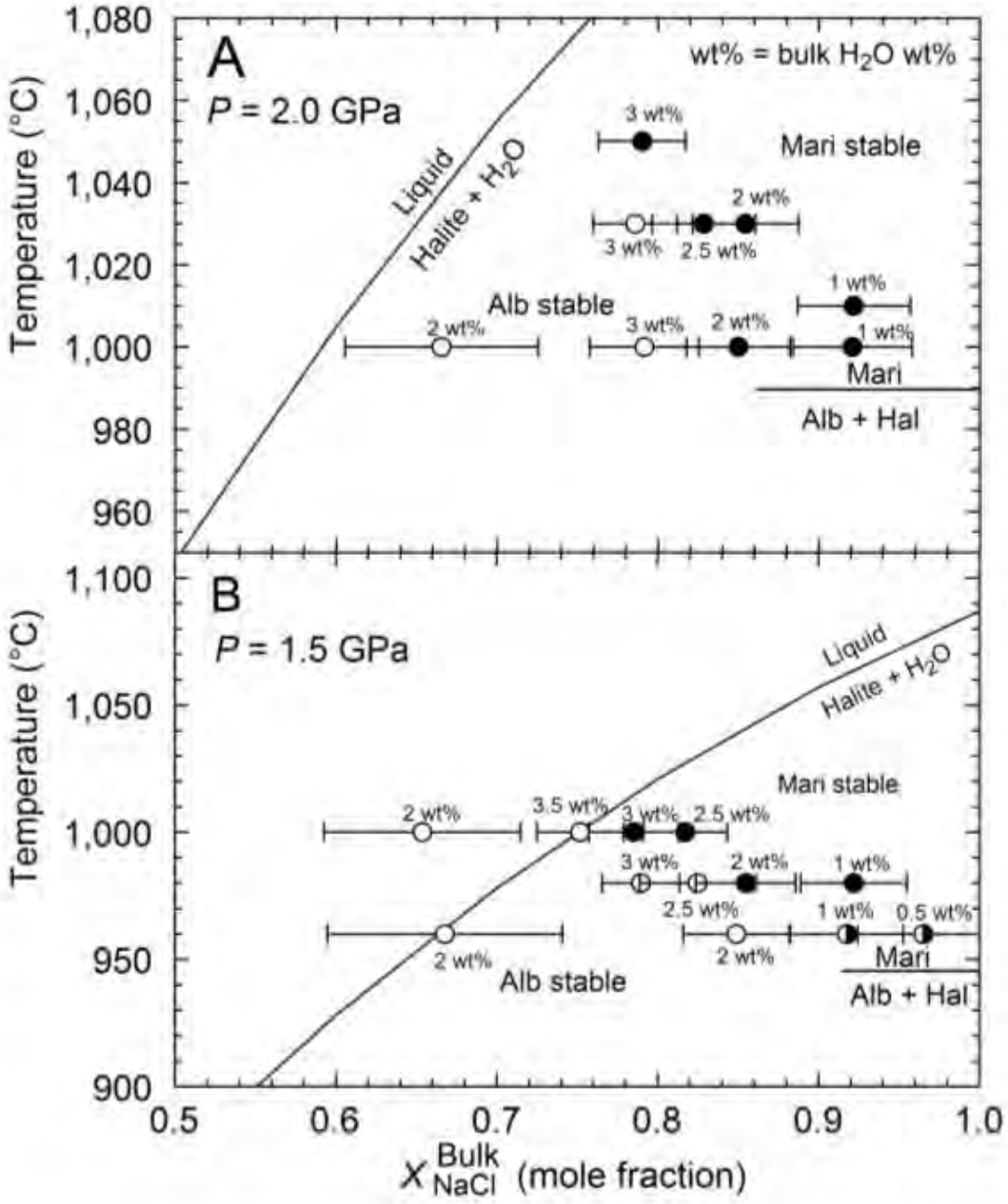

701
702
703
704

This is a preprint, the final version is subject to change, of the American Mineralogist (MSA)
Cite as Authors (Year) Title. American Mineralogist, in press.
(DOI will not work until issue is live.) DOI: http://dx.doi.org/10.2138/am-2017-6132

Figure 3.

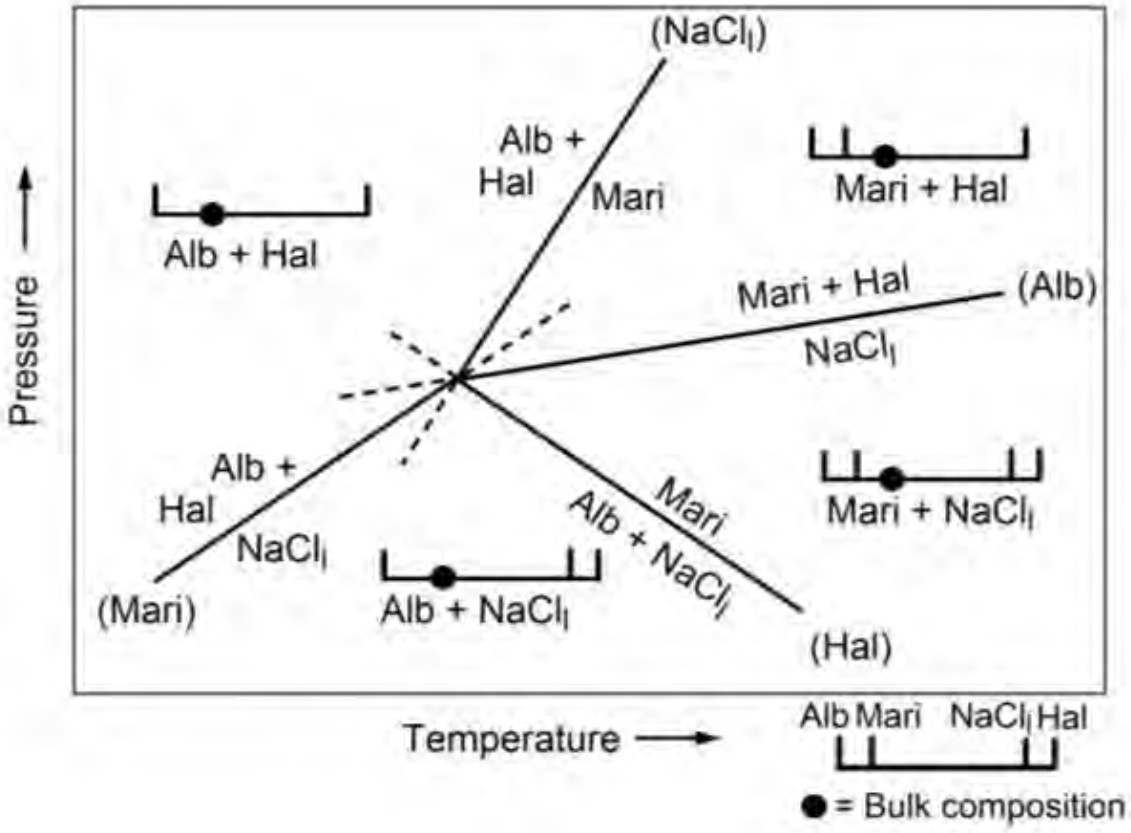

711 Figure 4.
712

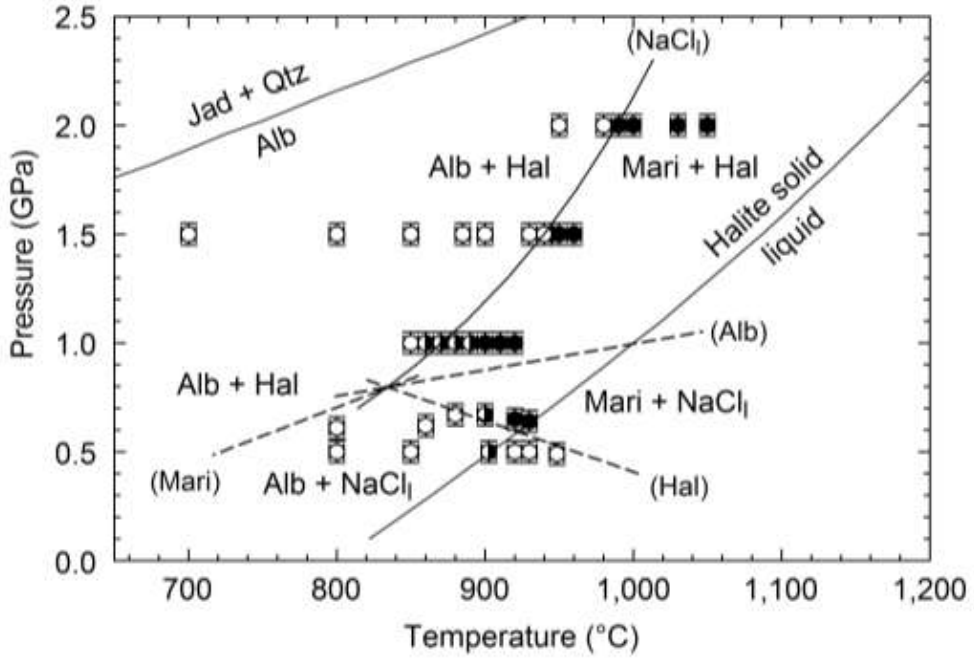

713
714
715 Figure 5.

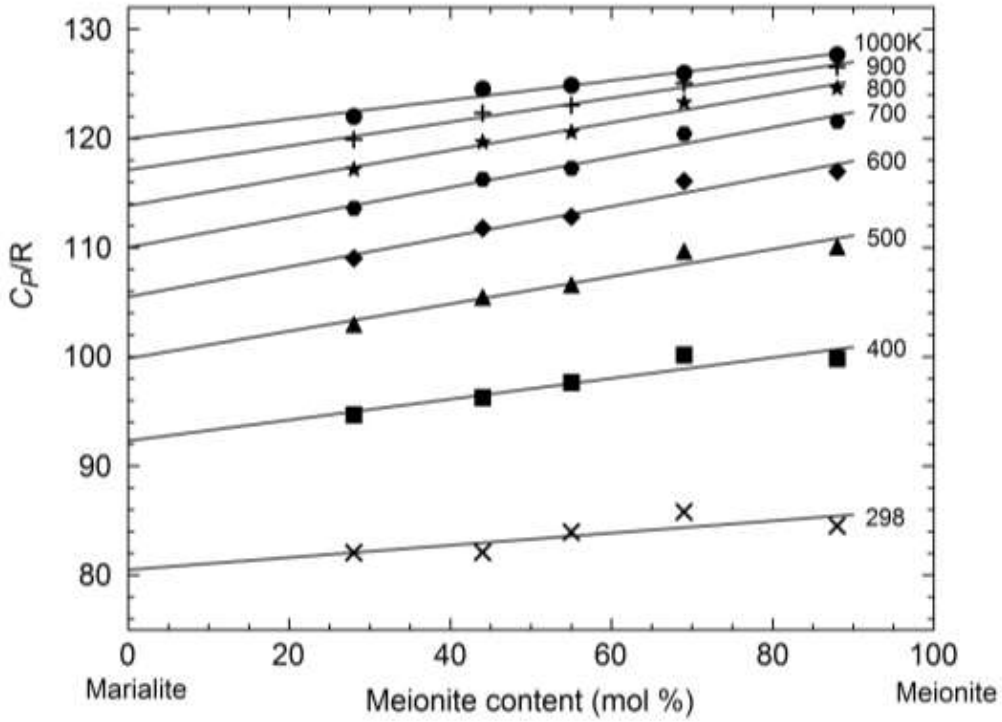

716
717

718 Figure 6. a,b
719

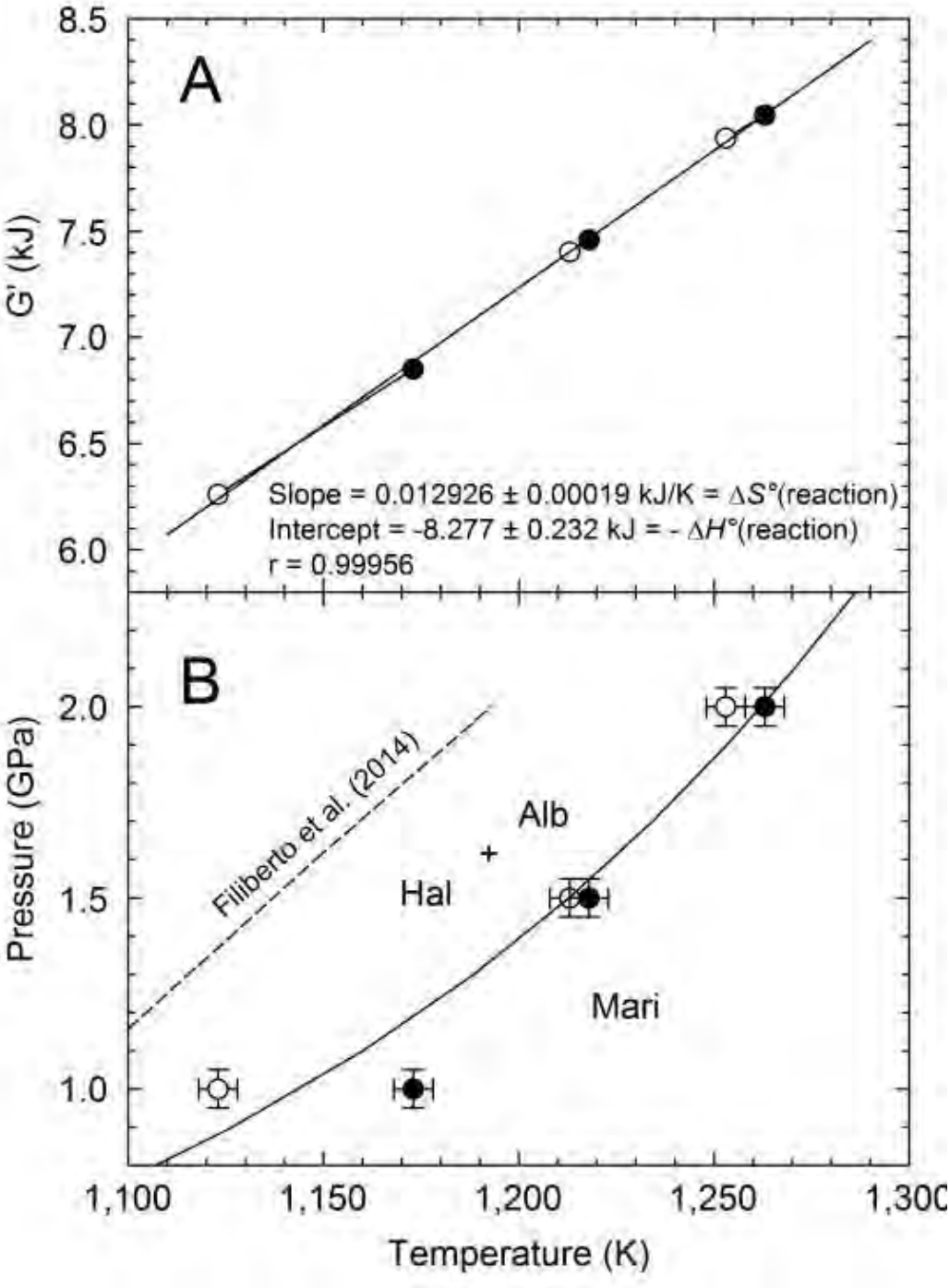

720
721
722

723 Figure 7.

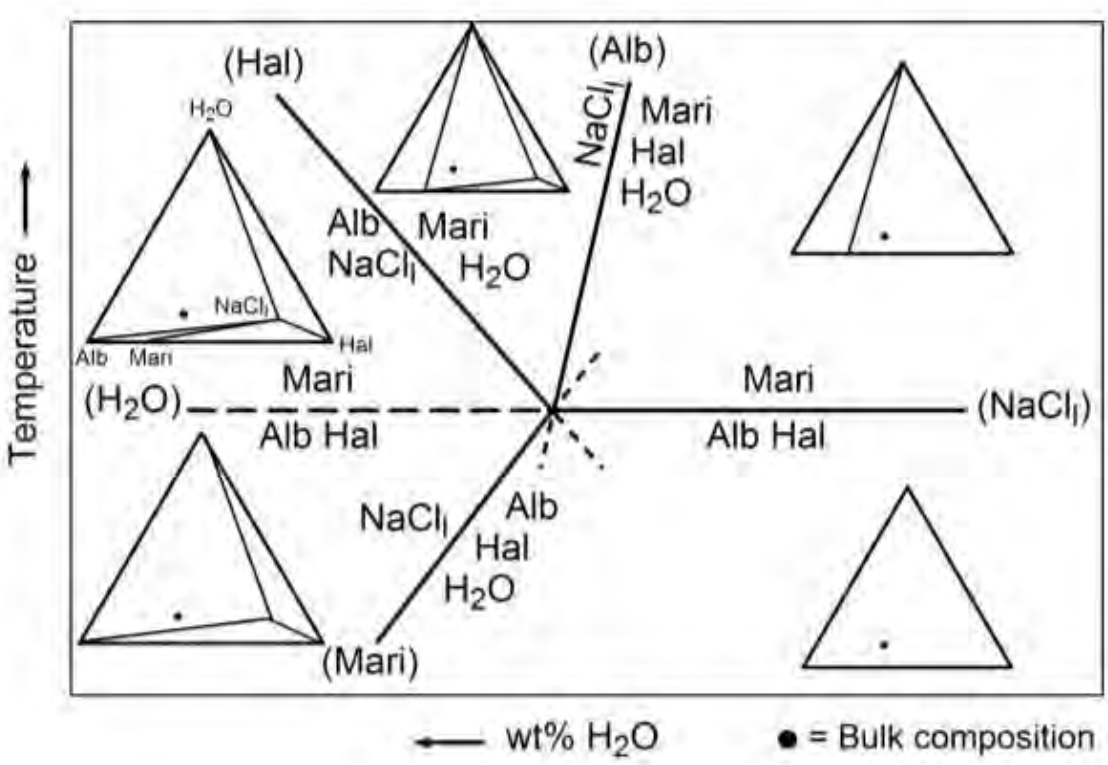

724
725
726
727

This is a preprint, the final version is subject to change, of the American Mineralogist (MSA)
Cite as Authors (Year) Title. American Mineralogist, in press.
(DOI will not work until issue is live.) DOI: http://dx.doi.org/10.2138/am-2017-6132

728 Figure 8. a,b
729

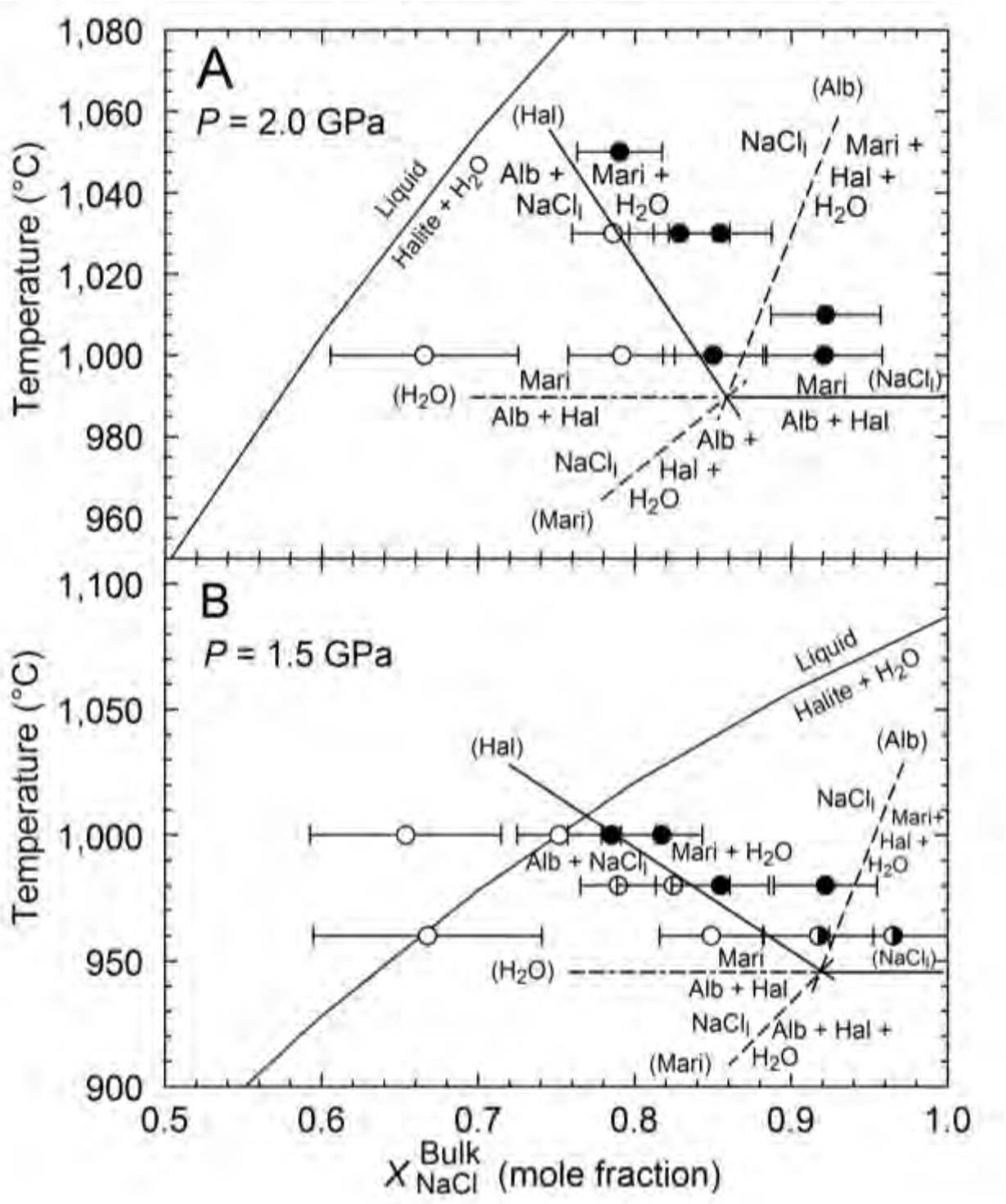

730
731
732

733 Figure 9.
734

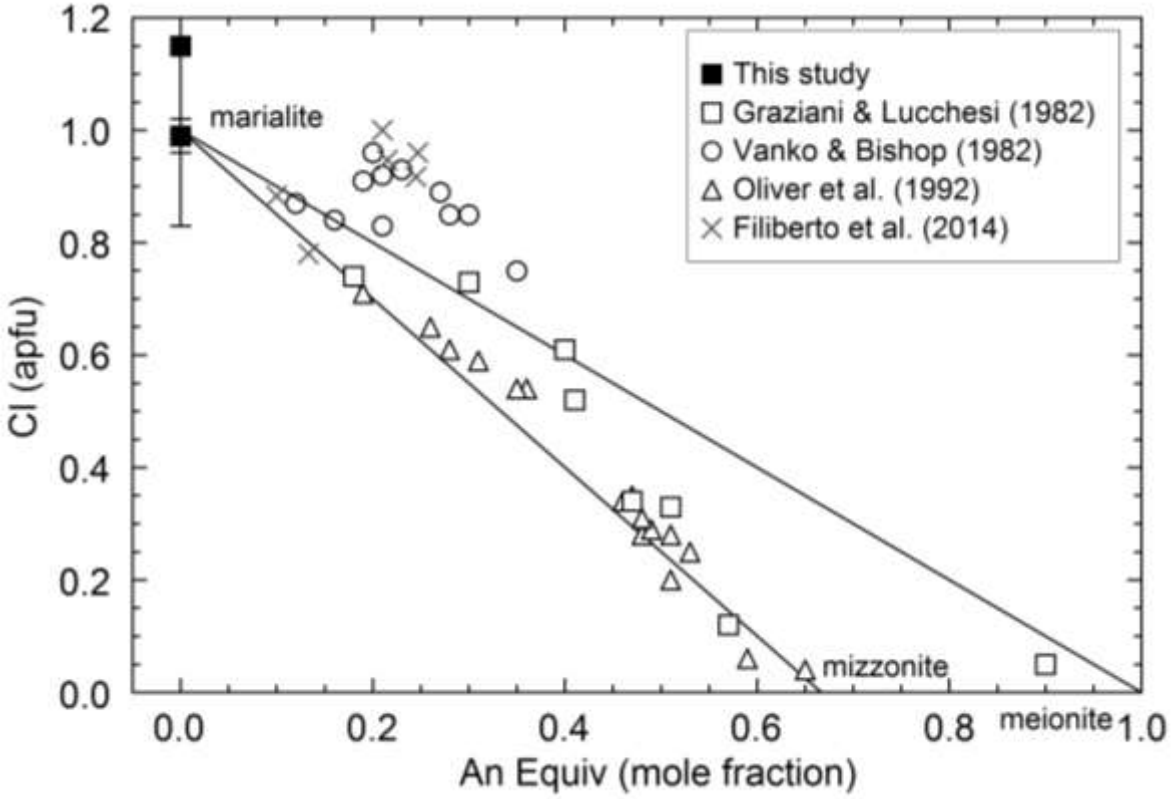

735
736
737